Spectroscopic and electronic structure properties of CdSe nanocrystals: Spheres and cubes

ARTICLE *in* PHYSICAL CHEMISTRY CHEMICAL PHYSICS · MARCH 2014

Impact Factor: 4.49 · DOI: 10.1039/c3cp55314k · Source: PubMed

2 AUTHORS, INCLUDING:

Vitaly Proshchenko
University of Wyoming
7 PUBLICATIONS **10** CITATIONS

SEE PROFILE

PCCP

PAPER

View Article Online
View Journal | View Issue

Cite this: *Phys. Chem. Chem. Phys.*, 2014, **16**, 7555

Spectroscopic and electronic structure properties of CdSe nanocrystals: spheres and cubes

Vitaly Proshchenko and Yuri Dahnovsky*

Received 17th December 2013,
Accepted 20th January 2014

DOI: 10.1039/c3cp55314k

www.rsc.org/pccp

In this work we study the electronic structure of Cd_mSe_m quantum dots of various sizes and different shapes such as spheres and cubes using DFT, TDDFT, and CIS methods. This work requires a careful computational analysis where a proper exchange–correlation functional has to be chosen to fit the experimental optical gap. We find some differences in the optical and HOMO–LUMO gap values between spheres and cubes. In general, the gaps for the cubes have higher values than those for the spheres. We also calculate optical absorption spectra using the data for energy levels and oscillator strengths for optical transitions. We find that DFT yields some discrepancy in the density of states for the spheres and cubes. However, the density of states calculated by TDDFT and CIS provide better agreement. The results of the calculation can be useful for quantum dots synthesized in laser ablation experiments.

I. Introduction

Nanocrystalline semiconductor nanoparticles or quantum dots (QDs) have been recently used as sensitizers in porous nanocrystalline solar cells.[1–5] The promising properties of QDs include higher absorption coefficients, and potentially increased stability due to their inorganic nature.[6] Another important feature in a QD is size-dependence of different physical properties such as electronic levels, vibrational frequencies, absorption coefficients, and relaxation rates (a phonon bottleneck).[5,7–10] The possible exploitation of quantum confinement effects such as increased photocurrent rate as a result of multiple exciton generation[6,17–22] from photons more than twice the band gap energy further stimulates the investigation of quantum dots as sensitizers. CdSe is an important and commonly used material for quantum dots and therefore, CdSe QDs have been intensively investigated by various computational methods. For example, Prezhdo *et al.* studied the effect of ligands on optical and electronic spectra where different ligands are capable of changing electronic levels.[7,8,10–12] In these works the computations were performed on VASP and Gaussian software codes with an original program that calculates the relaxation electron–phonon constants from the excited electronic states as well as oscillator strengths for DFT calculations. In this research we study CdSe nanocrystals with no ligands to analyze some experimental data where laser ablation[14–16] methodologies were used to synthesize nanocrystals in a vacuum. The temperature and pressure dependencies of the energy gap for CdSe clusters were reported in ref. 24. As pointed out by Chelikowsky and co-workers[25] e–e correlations are also very important for electronic properties of small clusters of Cd_nSe_m ($n \neq m$). Additionally Sarkar *et al.*[26] studied the effect of uneven numbers of atoms m and n and found that the most stable configuration is for $m = n$. The same conclusion was also drawn using the tight-binding approximation. For very small clusters where $n = m = 3$, 6 electron correlations can be correctly accounted for within GW + Bethe–Salpeter calculations as concluded by Noguchi *et al.*[30]

To explain the experimental absorption spectra of CdSe quantum dots it is important to employ more advanced computational methods such as TDDFT, EOM-CCSD, CIS(D), and CIS because they include electron–hole interactions, that are absent in DFT. As an advantage, these methods additionally provide the oscillator strengths for excited electronic levels. The oscillator strengths determine the intensity of an absorption line defined as follows:[31]

$$f_{mn}^{x} = \frac{2m\omega}{\hbar}|\langle m|x|n\rangle|^2. \quad (1)$$

Consequently, optical and HOMO–LUMO gaps, absorption spectra, and the density of states can be found from the correct procedure using TDDFT and CIS computational methods. These results are compared with those from the DFT calculations for various sizes and shapes (spheres and cubes) of CdSe quantum dots by using a Gaussian 09 software package.[33] Quantum dots of the spherical and cubic shapes are depicted in Fig. 1(a) and (b), respectively.

Department of Physics and Astronomy, University of Wyoming, 3905, 1000 E. University Avenue, Laramie, WY 82071, USA. E-mail: yurid@uwyo.edu

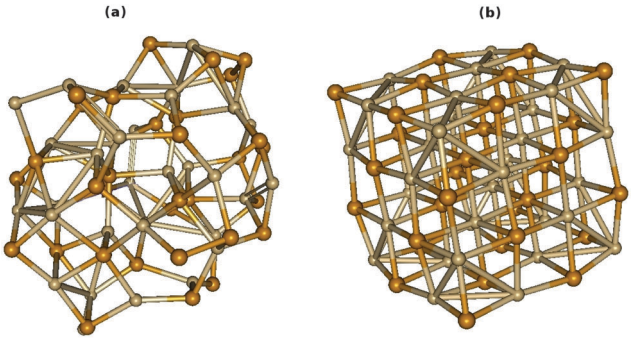

Fig. 1 $Cd_{32}Se_{32}$ quantum dots of (a) spherical and (b) cubic shapes.

II. Calculation details

Electronic structures of Cd_mSe_n (we have studied $m = n$ only) quantum dots have been calculated for spherical (m = 10,16,24,32,82) and cubic shapes (m = 4,32,108). Such a number of atoms in a nanoparticle provides a range of sizes from 1.0 to 2.0 nm for spheres and from 0.5 to 2.5 nm for cubes. For the small spheres there are experimental data that we have analyzed. These data are published in ref. 27–29. We would also like to cite a computational work for Cd_mSe_m with m = 33 (ref. 11) where a similar sized nanocrystal was considered. In this work we study m = 32 for spheres and cubes. One of the goals of this research is to compare the results of the calculations for spheres and cubes. The only size where these two different shapes intersect is m = 32. Spherical QDs with no ligands were experimentally studied by laser ablation in ref. 14. It was shown that the binding energies of $Cd_{32}Se_{32}$ are infinitesimally smaller than those of $Cd_{33}Se_{33}$ and $Cd_{34}Se_{34}$ (the binding energy difference is less than 0.03 eV). The accuracy of the electronic structure calculations is much smaller. Moreover, as was discussed in ref. 32 $Cd_{32}Se_{32}$ clusters computationally are more stable than $Cd_{33}Se_{33}$ and $Cd_{34}Se_{34}$ QDs if ligands are not taken into account.

To find energy states and levels we have used a Gaussian software package[33] employing various computational methods. The initial calculations have been performed by using DFT with the different exchange–correlation functionals, B3LYP, B1LYP, BHandH, BHandHLYP, Hybrid1, Hybrid2, and Hybrid3. The definition of Hybrid1, 2, 3 functionals is discussed below. Different exchange–correlation functionals provide different energy gap values. To determine the most suited exchange functional we have used gap values computed by the TDDFT method and compared them with the available experimental data. We have found that the standard built-in exchange functionals do not reproduce the experimental values. Therefore, we have decided to make up new hybrid functionals, called Hybrid1, 2, 3 in this work, where the fraction of the exchange–correlation and Hartree–Fock contributions is variable. The dependence of the optical gap on a computational method is shown in Fig. 2. A hybrid exchange–correlation functional defined as "User-Defined Models" provided from the Gaussian official webpage has the general form:[34]

$$P_2E_X^{HF} + P_1(P_4E_X^{Slater} + P_3\Delta E_X^{non\text{-}local}) + P_6E_C^{local} + P_5\Delta E_C^{non\text{-}local}, \quad (2)$$

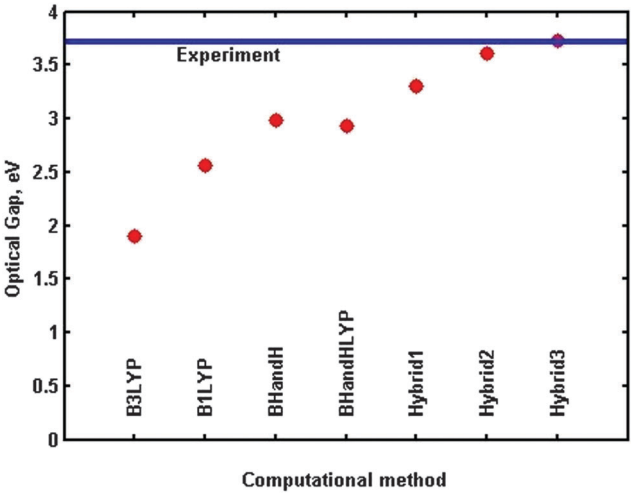

Fig. 2 Computed optical gap for a $Cd_{10}Se_{10}$ QD depending on the exchange–correlation functional. In addition, we have found that the experimental value matches the results obtained from the coupled cluster calculations.

where $P_{1,2,3,4,5,6}$ are adjustable coefficients. In eqn (2) the energies with subscript X denote an exchange part of the functional while the subscript C stands for the correlations. The superscripts local and non-local describe the local (LDA) and non-local (GGA) parts of the functional. In eqn (2) the non-local exchange and correlation functionals are B and LYP, respectively.[34] The coefficients P are variables that can enforce one part with respect to the other. For Hybrid1, 2, 3 we have changed only P_2 enhancing the Hartree–Fock part because the Hartree–Fock contribution increases the gap that is necessary in our calculations to fit experimental data and also the coupled cluster calculations. Thus, we have chosen the following set of coefficients: P_2 = 0.7, 0.8, 0.84 for Hybrid1, 2, 3, respectively and the coefficients P_1 = 1, P_3 = 0.5, P_4 = 0.5, P_5 = 1, and P_6 = 0 are the same for all three hybrid functionals.

The next step is to choose a proper basis set. For the optimal basis set we have used a LANL2dz basis set, which we have employed for all calculations. This basis set is very popular for the problem under investigation and has been broadly used for the description of quantum dots.[10,12] The pseudopotential was chosen to be LANL2. We have used the same basis set, functional and pseudopotential for the DFT and TDDFT (CIS) calculations. In addition we have also used a B3LYP functional for DFT calculations.

The QDs of spherical shape were cut out of a wurtzite crystal with successive optimization. The experimental X-ray diffraction experiments indicated that CdSe QDs have only the wurtzite structure.[13] We chose a cubic shape for the nanocrystals according to the following procedure before optimization: the first cube was selected as a one unit cell with eight atoms, the second cube contains 8 unit cells, the third has 27 unit cells. For small spherical clusters the optimization has been checked for the global minimum using the Coalescence Kick method.[35]

To find the optical spectral function and density of states we have employed TDDFT and CIS computational methods. In this

work we do not study a spin–orbit effect. This is a general approximation used by many authors (see *e.g.*, ref. 11, 23 and 25).

III. Results and discussion

There are many ways to calculate an energy gap for different QD sizes. In general, investigators can use the DFT method and adjust an exchange–correlation functional to fit experimental values. However, the experimental gap is usually obtained from optical experiments, and therefore, HOMO–LUMO and optical gaps can be different because some transitions can have vanishing oscillator strengths (see eqn (1)). Moreover, DFT does not include electron–hole interactions. In this case, it is more appropriate to use the TDDFT or CIS computational methods where all the problems mentioned above are taken into account. In the previous section (see also Fig. 2) we have described the procedure of how to choose a hybrid exchange–correlation functional that fits the experimental value of the optical gap in the best way, that is Hybrid3. Now we compare two different DFT calculations, one with the Hybrid3 exchange–correlation functional and another with the B3LYP functional. The former has been chosen to fit the experimental optical gap for different QD sizes. As shown in Fig. 3 we have found that the DFT HOMO–LUMO gap with the Hybrid3 functional is much greater than that with the B3LYP functional. However, the optical gap is much better described with Hybrid3. Such a comparison indicates that the TDDFT or CIS calculations with a B3LYP functional yield much lower values of the gap shown in Fig. 2. TDDFT and CIS yield lower gap values compared to the DFT results because the negative electron–hole interaction included in TDDFT and CIS methods decreases the energy gap. Thus, for the description of optical spectra TDDFT and CIS seem to us to be more reliable than DFT with a B3LYP functional because the former two methods include electron–hole interactions.

As soon as the proper exchange–correlation potential is chosen (Hybrid3) we are able to find the size-dependence of the optical gap for spheres and cubes using the TDDFT and CIS computational methods. We employ the two different independent methods to be sure that in the case of close dependencies the computational results can be trusted. In Fig. 4 the size-dependence of the optical gap obtained from the TDDFT, CIS, and tight-binding approximation calculations[27,28] was compared with the experimental data[29] for (a) spheres and (b) cubes (there are no tight-binding calculations available, and we have not found experimental data either). The TDDFT and CIS methods provide excellent agreement with the experimental dependencies and tight-binding results for spheres. Thus, we conclude that both methods, TDDFT and CIS, are reliable to provide the correct description of QD electronic structures. We have also applied the same method to the calculations of optical gaps for cubic QDs. We have found that there is an excellent agreement between the results obtained by the two methods for larger cubic and spherical QD sizes with some discrepancy for smaller cubes.

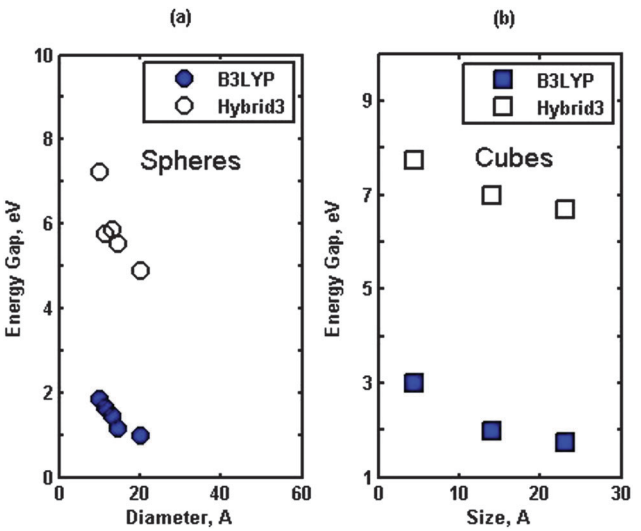

Fig. 3 Size dependence of HOMO–LUMO gaps in the DFT calculations with the B3LYP and Hybrid3 functionals for (a) spherical and (b) cubic QDs.

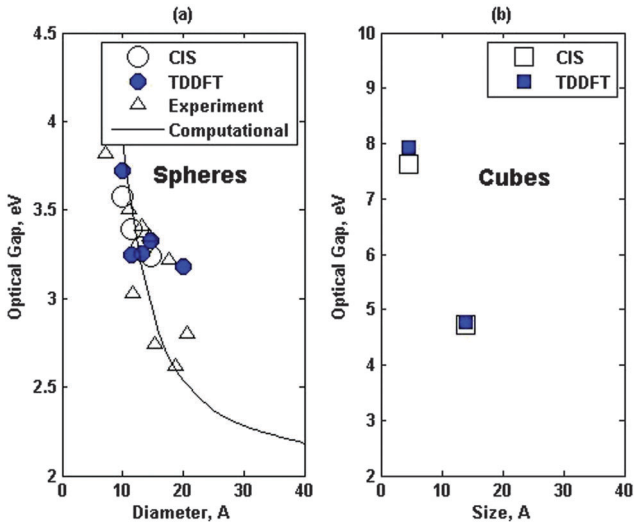

Fig. 4 Size-dependence of the optical gap in the TDDFT, CIS, and tight-binding calculations for (a) spheres and (b) cubes.

In Fig. 5 we present the size-dependence of the optical and HOMO–LUMO gaps for (a) spheres and (b) cubes in the TDDFT and CIS calculations. It becomes clear that the optical gap is larger than the HOMO–LUMO gap for the spheres and cubes. For the spheres there is a difference in the gaps of about 1.5 eV. The difference between the optical and dark (HOMO–LUMO) energy gaps can be explained by the low values of the oscillator strengths for the near-gap transitions. It looks counter intuitive at first glance that the energy gap increases with the size of a cubic cluster (see Fig. 5b). We have the following qualitative explanation: the sizes of cubes are still small, the first cube contains only 8 atoms; and the e–e^{-} interaction is important as pointed out by Chelikowsky and coworkers.[25] Therefore, a simple quantum mechanical model like a particle-in-the-box is not applicable for small systems with strong e–e interactions. We note the B3LYP functional provides excellent agreement with the TDDFT and CIS calculations as shown Fig. 5a.

It is important to compare the size-dependencies of the (a) optical and (b) HOMO–LUMO gaps for quantum dots of the same size but different shape. As shown in Fig. 6a, the optical

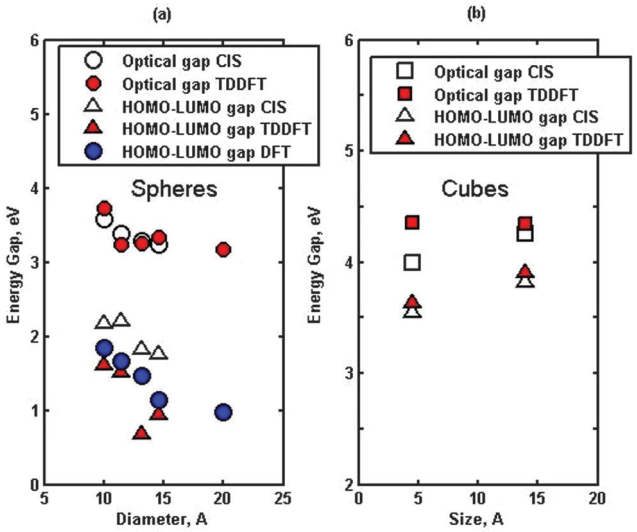

Fig. 5 Size-dependencies of the optical and HOMO–LUMO gaps for (a) spheres (the TDDFT, CIS, and DFT calculations for HOMO–LUMO gaps) and (b) cubes (the CIS and TDDFT calculations for all gaps). For the DFT method the B3LYP functional has been chosen.

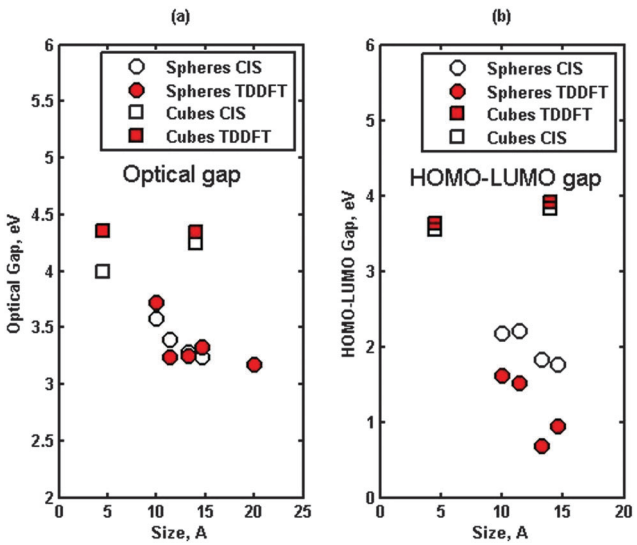

Fig. 6 Size-dependencies of the (a) optical and (b) HOMO–LUMO gaps for spheres and cubes in the CIS and TDDFT calculations.

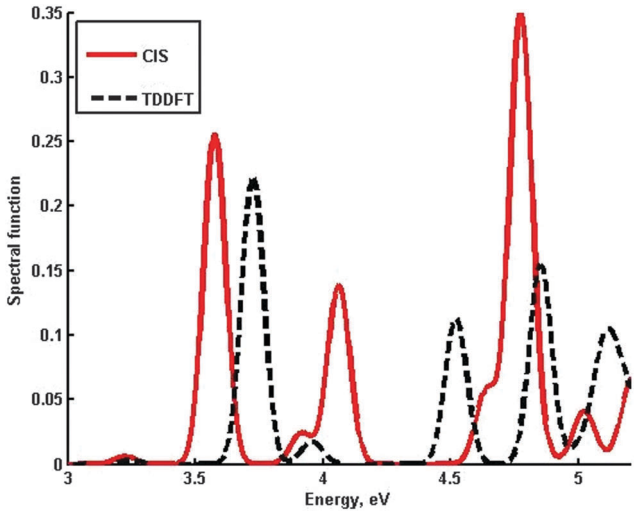

Fig. 7 Spectral functions for a spherical $Cd_{10}Se_{10}$ quantum dot calculated by the TDDFT and CIS methods.

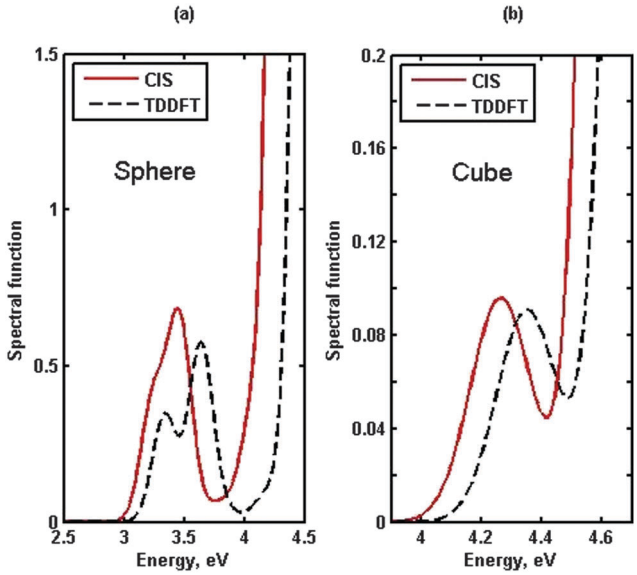

Fig. 8 Spectral functions for (a) spherical and (b) cubic $Cd_{32}Se_{32}$ quantum dots calculated by the TDDFT and CIS methods.

gap for the cubes is always larger than for the spheres. The discrepancy increases for larger QD sizes. For HOMO–LUMO gaps (see Fig. 6b) the picture is similar but there are some differences: (a) the gaps lie in the lower range of energies both for cubes and spheres, (b) there is a significant difference in values for the spheres and cubes, for the spheres the energy is below 2.0 eV for larger sizes while for cubes it is larger than 3.5 eV, and (c) the cube gaps are growing with size while they reduce for the spheres. We believe that such growth is true only for small clusters due to the strong e–e correlation effects. For larger clusters, which we have not calculated in this work, the gap will decrease in accordance with the-particle-in-a box model.

As is shown in Fig. 7 the CIS *ab initio* method provides good agreement with the results obtained by TDDFT.

Besides optical and HOMO–LUMO gaps we have also calculated optical absorption spectra using the data for energy levels and oscillator strengths for optical transitions. In Fig. 8 the spectral function calculated in the TDDFT and CIS methods is presented for (a) spherical and (b) cubic $Cd_{32}Se_{32}$ quantum dots. For spherical QDs the two different computational methods provide similar spectral functions shifted from each other by 0.3 eV. We also observe two absorption lines for spherical QDs where the first peak could be identified as $1S(e) - 1S_{3/2}(h)$ transition and the second peak as $1S(e) - 2S_{3/2}(h)$ in the effective mass approximation.[37] In the case of the cubic QDs the absorption spectrum differs from the spectral

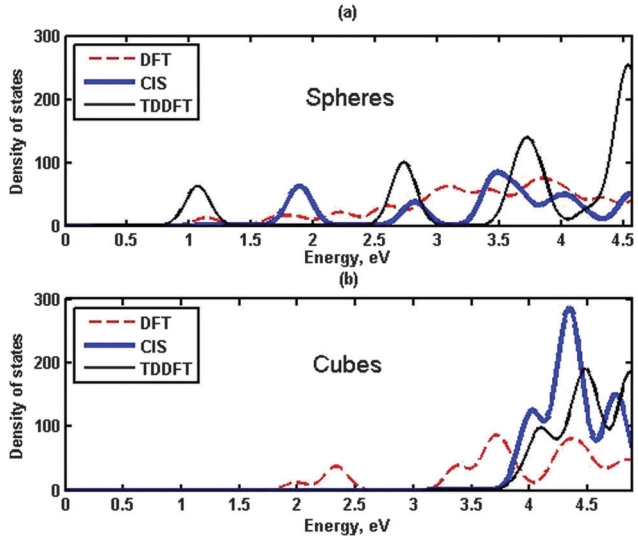

Fig. 9 Density of states for (a) spherical and (b) cubic $Cd_{32}Se_{32}$ quantum dots calculated by the TDDFT, CIS and DFT methods.

function for the spheres. Indeed, we observe only one peak for the cubes at low energies while the spheres exhibit two distinct peaks. The discrepancy in the spectral functions calculated by the TDDFT and CIS methods for the cubes is much smaller than for the spheres. In general, spherical QDs exhibit higher absorption numbers than cubic QDs. The cubes absorb in a higher frequency range. The value of the gap for the spheres is lower than the gap for the cubes as shown in Fig. 8.

It is also important to find the spectral dependencies of all states including the dark ones. For this we calculate the density of states for (a) spheres and (b) cubes. The results are depicted in Fig. 9 where the density of states have been calculated with the DFT, TDDFT, and CIS methods. For the calculations using TDDFT and CIS we have included both singlet and triplet states. For the DFT calculations we have chosen a B3LYP exchange–correlation functional. As shown in Fig. 9(a), the CIS and TDDFT provide similar but slightly shifted curves with some difference in amplitude. The curves are much closer in the case of the cubic QDs (see Fig. 9(b)). It is hard to say which method, TDDFT, CIS or DFT, is better for a spherical shape. In general, all methods provide slightly different dependencies. However, for the cubes TDDFT and CIS yield closer curves while the DFT calculations reveal much smaller gaps (about 2 eV) compared to those of TDDFT and CIS (4 eV). For spheres and cubes the DFT curve is lower than the TDDFT and CIS graphs.

IV. Conclusions

In this research we have computationally studied optical and energy (the density of states) spectra for Cd_mSe_m clusters of various sizes and shapes, *i.e.*, spheres and cubes. For electronic structure calculations we have used a higher level than the DFT methods such as CIS, and then compared the results obtained with the DFT calculations and the available experimental data. The experimental gap cannot be identified as a HOMO–LUMO gap because some transitions might have vanishing oscillator strengths (see eqn (1)). We have been very careful in the methodology, especially in choosing a proper exchange–correlation functional and found that Hybrid3 is the best functional to describe the experimental optical gap value (see Fig. 2). Using TDDFT and CIS methods we have calculated the optical gaps for cubes and spheres as shown in Fig. 4. The calculations for the spheres have revealed excellent agreement between the two methods as well as the experimental data. For cubes the excellent agreement between the CIS and TDDFT computations has been observed only for the larger sizes. Despite the absence of experimental data for optical spectra, the calculated dependencies can be considered as a prediction and therefore, could be useful for future experiments. Besides the computations of the optical gaps, we have also calculated optical absorption spectra using the data for energy levels and oscillator strengths for optical transitions. The results are depicted in Fig. 7 and 8. As shown in Fig. 7 the optical spectra calculated by the CIS method yields the curve that is in good agreement with TDDFT calculations. Then we have used only CIS and TDDFT and found that the two different computational methods provide similar agreement in the profile spectral functions shifted by about 0.3 eV for spherical QDs as shown in Fig. 8. We have also observed two distinctive peaks (bands) at lower frequencies where the first peak could be identified as $1S(e) - 1S_{3/2}(h)$ transition and the second peak as $1S(e) - 2S_{3/2}(h)$ in the effective mass approximation for larger clusters (it is obvious that the effective mass approximation is not a good approximation for small and mid-size clusters).[37] For the cubes the picture is similar. The discrepancy in the spectral functions calculated by the TDDFT and CIS methods for the cubes is much smaller than for the spheres. The spectrum for cubes is shifted to a higher frequency range. The values of the gap for the cubes are higher than for the spheres as shown in Fig. 8.

The size dependencies of optical and HOMO–LUMO gaps for cubes and spheres are presented in Fig. 5 and 6. As depicted in Fig. 5b the HOMO–LUMO gap increases with cube size. At first glance it contradicts the simple particle-in-the-box model. We believe that this simple model does not work for small clusters where the e–e interaction is strong (see *e.g.*, ref. 25). Indeed, the smallest cube contains only eight atoms. Such behavior can be different for QDs. For instance, the experimental data for PbS clusters show that the gap oscillates with cluster size.[36] We believe that for small clusters, size dependencies of a HOMO–LUMO gap are unpredictable. This is probably connected to the strong e–e correlation effects. There is a difference in gaps for spheres and cubes. In general the gap values for spheres are smaller than for cubes. In all dependencies the optical gaps are higher than the HOMO–LUMO gaps. The dark states are described by the density of states, which has been calculated by the DFT, TDDFT, and CIS methods (see Fig. 9). The density of states calculations include both singlet and triplet states. The triplet states are essential for spheres in the whole range of energies, that is why the HOMO–LUMO gap is much smaller than the optical one. For the cubes the picture is different, the triplet states contribute most at larger energies and the

HOMO–LUMO gap is approximately the same as the optical one in the TDDFT and CIS calculations (see Fig. 8). In general, the HOMO–LUMO gaps for the cubes are larger than for the spheres.

In addition, we have studied the stability of cubes and spheres. The difference in the total energies between the spherical and cubic clusters of $(CdSe)_{32}$ calculated by CIS is

$$E^{tot}_{spheres} - E^{tot}_{cubes} = -0.35 \text{ eV}. \quad (3)$$

It seems to us that this is a very small difference taking into account that the number of atoms is 64, *i.e.*, large. The excited states or optical spectra could have larger differences that can be explained by the polarizing nature of d-orbitals participating in the bonding. Indeed, even if the atoms for both shapes can be approximately at the same distances, the angles of the directed d-orbitals can be different for the two shapes, and therefore, the matrix elements (overlaps and Coulomb integrals) can be substantially varied.

The DFT method was tested in ref. 11. The authors of this work found that DFT provides the absorption spectra close to those of the TDDFT. In addition, optical spectra were computed using only DFT with the corresponding calculation of oscillator strengths that required additional programing. We are currently working on an implementation that will allow for the calculation of the optical spectra using DFT. However, our calculations for the density of states show the discrepancies between the TDDFT-CIS and DFT methods where in the latter we have used a B3LYP exchange–correlation functional. For the spheres, as shown in Fig. 9 the positions of the peaks in the density of states are close to those of the TDDFT/CIS ones. For cubes they are shifted. Thus, we conclude that the DFT method probably can be used for the density of states calculations but with some care.

Acknowledgements

This work was supported by a grant (No. DEFG02-10ER46728) from the Department of Energy to the University of Wyoming and by the University of Wyoming School of Energy Resources through its Graduate Assistantship program.

References

1 A. Kongkanand, K. Tvrdy, K. Takechi, M. Kuno and P. V. Kamat, *J. Am. Chem. Soc.*, 2008, **130**, 4007.
2 H. J. Lee, J.-H. Yum, H. C. Leventis, S. M. Zakeeruddin, S. A. Haque, P. Chen, S. I. Seok, M. Grätzel and M. K. Nazeeruddin, *J. Phys. Chem. C*, 2008, **112**, 11600.
3 M. T. Spitler and B. A. Parkinson, *Acc. Chem. Res.*, 2009, **42**, 207.
4 O. V. Prezhdo, *Acc. Chem. Res.*, 2009, **42**, 2005.
5 O. V. Prezhdo, *Chem. Phys. Lett.*, 2008, **460**, 1.
6 A. J. Nozik, *Chem. Phys. Lett.*, 2008, **457**, 3.
7 S. V. Kilina, D. S. Kilin and O. V. Prezhdo, *ACS Nano*, 2009, **3**, 93.
8 S. V. Kilina, D. S. Kilin, C. F. Craig and O. V. Prezhdo, *J. Phys. Chem. C*, 2007, **111**, 487.
9 C. M. Isborn, S. V. Kilina, X. Li and O. V. Prezhdo, *J. Phys. Chem. C*, 2008, **112**, 18291.
10 S. V. Kilina, S. Ivanov and S. Tretiak, *J. Am. Chem. Soc.*, 2009, **131**, 7717.
11 S. V. Fischer, A. M. Crotty, S. V. Kilina, S. A. Ivanov and S. Tretiak, *Nanoscale*, 2012, **4**, 904.
12 T. M. Inerbaev, A. E. Masunov, S. I. Khondaker, A. Dobrinescu, A.-V. Plamad and Y. Kawazoe, *J. Chem. Phys.*, 2009, **131**, 044106.
13 S. Neeleshwar, C. L. Chen, C. B. Tsai and Y. Y. Chen, *Phys. Rev. B: Condens. Matter Mater. Phys.*, 2005, **71**, 201307(R).
14 A. Kasuya, R. Sivamohan, Y. Barnakov, I. Dmitruk, T. Nirasawa, V. R. Romanyuk, V. Kumar, S. V. Mamykin, K. Tohji, B. Jeyadevan, K. Shinoda, T. Kudo, O. Terasaki, Z. Liu, R. V. Belosludov, V. Sundararajan and Y. Kawazoe, *Nat. Mater.*, 2004, **3**, 99.
15 S. Horoz, L. Lu, Q. Dai, J. Chen, B. Yakami, J. M. Pikal, W. Wang and J. Tang, *Appl. Phys. Lett.*, 2012, **101**, 223902.
16 Q. Dai, J. Chen, L. Lu, J. Tang and W. Wang, *Nano Lett.*, 2012, **12**, 4187.
17 R. D. Schaller and V. I. Klimov, *Phys. Rev. Lett.*, 2004, **92**, 186601.
18 A. L. Efros, V. A. Kharchenko and M. Rosen, *Solid State Commun.*, 1995, **93**, 281.
19 A. J. Nozik, *Annu. Rev. Phys. Chem.*, 2001, **52**, 193.
20 R. J. Ellingson, M. C. Beard, J. C. Johnson, P. Yu, O. I. Micic, A. J. Nozik, A. Shabaev and A. L. Efros, *Nano Lett.*, 2005, **5**, 865.
21 M. C. Beard, K. P. Knutsen, P. R. Yu, J. M. Luther, Q. Song, W. K. Metzger, R. J. Ellingson and A. J. Nozik, *Nano Lett.*, 2007, **7**, 2506.
22 A. Piryatinski and K. A. Velizhanin, *J. Chem. Phys.*, 2010, **133**, 084508.
23 S. Kilina, K. A. Velizhanin, S. Ivanov, O. V. Prezhdo and S. Tretiak, *ACS Nano*, 2012, **6**, 6515.
24 H. Kamisaka, S. Kilina, K. Yamashita and O. V. Prezhdo, *J. Phys. Chem.*, 2008, **112**, 780.
25 M. Lopez del Puerto, M. L. Tiago and J. R. Chelikowsky, *Phys. Rev. B: Condens. Matter Mater. Phys.*, 2008, **77**, 045404.
26 P. Sarkar and M. Springborg, *Phys. Rev. B: Condens. Matter Mater. Phys.*, 2003, **68**, 235409.
27 S. Baskoutas and A. F. Terzis, *J. Appl. Phys.*, 2006, **99**, 013708.
28 G. Pellegrini, G. Mattei and P. Mazzoldi, *J. Appl. Phys.*, 2005, **97**, 073706.
29 W. Yu, L. Qu, W. Guo and X. Peng, *Chem. Mater.*, 2003, **15**, 2854.
30 Y. Noguchi, O. Sugino, M. Nagaoka, S. Ishii and K. Mohno, *J. Chem. Phys.*, 2012, **137**, 024306.
31 A. S. Davidov, *Quantum Mechanics*, Pergamon Press, New York, 1976.
32 K. A. Nguyen, R. Pachter and P. N. Day, *J. Chem. Theory Comput.*, 2013, **9**, 3581.
33 M. J. Frisch, G. W. Trucks, H. B. Schlegel, G. E. Scuseria, M. A. Robb, J. R. Cheeseman, G. Scalmani, V. Barone, B. Mennucci, G. A. Petersson, H. Nakatsuji, M. Caricato, X. Li, H. P. Hratchian, A. F. Izmaylov, J. Bloino, G. Zheng, J. L. Sonnenberg, M. Hada, M. Ehara, K. Toyota, R. Fukuda,

J. Hasegawa, M. Ishida, T. Nakajima, Y. Honda, O. Kitao, H. Nakai, T. Vreven, J. A. Montgomery, Jr., J. E. Peralta, F. Ogliaro, M. Bearpark, J. J. Heyd, E. Brothers, K. N. Kudin, V. N. Staroverov, R. Kobayashi, J. Normand, K. Raghavachari, A. Rendell, J. C. Burant, S. S. Iyengar, J. Tomasi, M. Cossi, N. Rega, J. M. Millam, M. Klene, J. E. Knox, J. B. Cross, V. Bakken, C. Adamo, J. Jaramillo, R. Gomperts, R. E. Stratmann, O. Yazyev, A. J. Austin, R. Cammi, C. Pomelli, J. W. Ochterski, R. L. Martin, K. Morokuma, V. G. Zakrzewski, G. A. Voth, P. Salvador, J. J. Dannenberg, S. Dapprich, A. D. Daniels, Ö. Farkas, J. B. Foresman, J. V. Ortiz, J. Cioslowski and D. J. Fox, *Gaussian 09, Revision A.1*, Gaussian, Inc., Wallingford CT, 2009.

34 http://www.gaussian.com/gtech/gur/kdft.htm.

35 B. Averkiev, Geometry and Electronic Structure of Doped Clusters via the Coalescence Kick Method, All Graduate Theses and Dissertations, Utah State University, 2009, paper 408, http://digitalcommons.usu.edu/etd/408.

36 S. Wu, H. Zeng and Z. A. Schelly, *Langmuir*, 2005, **21**, 686.

37 A. I. Ekimov, F. Hache, M. C. Schanne-Klein, D. Ricard, C. Flytzanis, I. A. Kudryavtsev, T. V. Yazeva, A. V. Rodina and A. L. Efros, *J. Opt. Soc. Am. B*, 1993, **10**, 100.